Palladium(II) complexes with pentafluorophenyl ligands: structures, C_6F_5 fluxionality by 2D-NMR studies and pre-catalysts for the vinyl addition polymerization of norbornene†

Frederik Blank,[a] Harald Scherer,[a] José Ruiz,*[b] Venancio Rodríguez[b] and Christoph Janiak*[a]

Received 7th December 2009, Accepted 4th February 2010
First published as an Advance Article on the web 5th March 2010
DOI: 10.1039/b925674a

The palladium(II) complex [Pd(C_6F_5)Cl(bpzm*)] (**5**) [bpzm* = bis(3,5-dimethylpyrazol-1-yl)methane] was characterized by ^{1}H,^{1}H-TOCSY, ^{1}H-NOE difference spectra, ^{1}H,^{19}F-HOESY and ^{13}C,^{1}H-HMBC 2D-NMR techniques. Chemical exchange of the methylene protons from ^{1}H,^{1}H-NOESY cross peaks and exchange of the *ortho*- and *meta*-fluorine atoms, respectively, from ^{19}F,^{19}F-EXSY cross peaks indicates that the Pd-bpzm* chelate ring boat-to-boat inversion occurs at a rate slower than the NMR time scale together with a concomitant change of the C_6F_5 atom positions. The presence of three ^{19}F-NMR signals for $2F_o : 1F_p : 2F_m$ of the C_6F_5 ligand for complexes [Pd(C_6F_5)Cl(tmeda)] (**1**) and [Pd(C_6F_5)Cl(bipy)] (**3**) (tmeda = *N*,*N*,*N*′,*N*′-tetramethylethylenediamine; bipy = 2,2′-bipyridine) is interpreted as being due to identical hemi-spaces above and below an apparent symmetry plane coinciding with the Pd-coordination plane instead of free ring rotation. The molecular structures of **1**, **3** and **5** from single-crystal studies suggest that the hindered C_6F_5 rotation is not limited to **5** but is also present in **1** and **3** due to ligand repulsion. Complexes [Pd(C_6F_5)Cl(tmeda)] (**1**), [Pd(C_6F_5)OH(tmeda)] (**2**), [Pd(C_6F_5)Cl(bipy)] (**3**), [Pd(C_6F_5)OH(bipy)] (**4**) and [Pd(C_6F_5)Cl(bpzm*)] (**5**) have been applied as pre-catalysts for the vinyl homopolymerization of norbornene in combination with the cocatalyst methylaluminoxane (MAO). Activities of more than 10^6 $g_{polymer}/(mol_{Pd}\ h)$ could be reached with these catalytic systems. Based on the spectrochemical series, pre-catalysts **1** and **2** with the pure σ-donor and more weakly bound aliphatic amine ligands showed higher polymerization activities than compounds **3–5** with modest π-accepting and stronger bound aromatic substituents. This is reasoned with a kinetic activation effect through a faster removal of the more weakly bound ligands upon reaction with MAO together with the chloro or hydroxo ligands to give the active, almost "naked" Pd^{2+} cations. For the activation mechanism, ^{1}H-, ^{13}C- and ^{19}F-NMR studies of the MAO activated complex **5** showed about 13% chlorine-to-methyl exchange for a molar Pd : Al ratio of 1 : 10. For **5** : MAO at a Pd : Al ratio of 1 : 100 abstraction of C_6F_5 takes place with a redox reaction giving Pd metal and C_6F_5-CH_3 in the absence of norbornene monomer.

Introduction

Norbornene (NB, bicyclo[2.2.1]hept-2-ene) can be polymerized by three different ways, each leading to its own polymer type (Scheme 1).[1–3] The best known polymerization route of norbornene is the ring-opening metathesis polymerization (ROMP), which leads to a polynorbornene (PNB) still containing double bonds in the polymer backbone.

In the vinyl or addition polymerization of NB, the bicyclic structure of the monomer remains intact, and only the double bond of the π component is opened.[1,2,3,4]

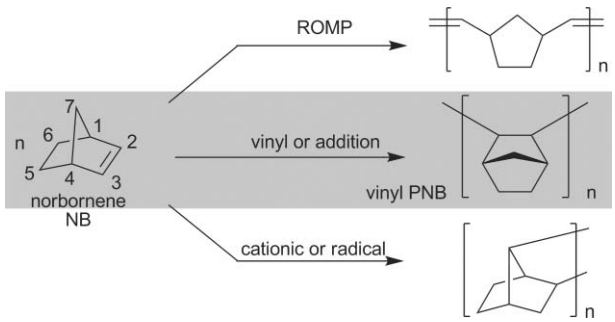

Scheme 1 Schematic representation of the three different types of polymerization of norbornene.

Vinyl PNB is of interest due to its good mechanical strength, heat resistivity, and optical transparency, for example, for deep ultraviolet photoresists, interlevel dielectrics in microelectronics applications, or as a cover layer for liquid-crystal displays.[5,6]

Films made from norbornene vinyl polymer are excellent in transparency and heat resistance and have unchanged viscoelastic and electric characteristics to high temperatures. Such a

[a]*Institut für Anorganische und Analytische Chemie, Universität Freiburg, Albertstr., 21, 79104, Freiburg, Germany. E-mail: janiak@uni-freiburg.de; Fax: +49 761 2036147; Tel: +49 761 2036127*
[b]*Departamento de Química Inorgánica, Facultad de Química, Universidad de Murcia, 30071, Murcia, Spain. E-mail: jruiz@um.es; Fax: +34 868 384148; Tel: +34 868 887455*

† Electronic supplementary information (ESI) available: Packing diagrams and supramolecular interactions for **1**, **3**, **5**, additional and enlarged NMR spectra. CCDC reference numbers 757345–757347. For ESI and crystallographic data in CIF or other electronic format see DOI: 10.1039/b925674a

film is suitable for a condenser or an insulator.[7] Furthermore, it shows a low water uptake, a small optical birefringence and dielectric loss.[8] The addition polymerization of substituted norbornenes was adopted for the preparation of electroactive polymers, in particular polymers designed as electro optical materials.[9] Bis(trifluoromethyl)carbinol-substituted polynorbornenes are promising materials for 157 nm photoresist resins.[10] The vinyl polymerization of NB uses catalytic systems based on titanium, chromium, iron, cobalt, copper, with recent emphasis on highly active nickel and palladium.[1–3]

Some examples of palladium(II) complexes bearing *N*,*N*-chelate ligands have been reported for the vinyl polymerization of norbornene.[1,2,3,5,11,12] At the same time, the pentafluorophenyl group with the ^{19}F nucleus is an excellent probe for molecular dynamics and for pre-catalyst activation mechanism by ^{19}F-NMR spectroscopy.[13] Generally, the species in MAO-activated Ni- or Pd-complexes and initiation steps for norbornene polymerization are not well known.[1,2,3,14] For the better defined co-catalytic system $B(C_6F_5)_3$ or $B(C_6F_5)_3/AlEt_3$ the activation process of the pre-catalyst $[Ph_3PCH_2C(O)CH_3]_2[Pd_2Cl_6]$ was followed by multinuclear (^1H, ^{13}C, ^{19}F, and ^{31}P) NMR investigations and points to the formation of molecular $PdCl_2$ which may represent the active species in the polymerization process.[15] Multinuclear (^{31}P and ^{19}F) NMR investigations on $[PdCl_2(dppe)]$ and $[PdCl_2(dppp)]$ in combination with $B(C_6F_5)_3$ and $B(C_6F_5)_3/AlEt_3$ suggest the formation of $[Pd(L)]^{2+}$ cations (L = dppe, 1,2-bis(diphenylphosphino)ethane; dppp, 1,3-bis(diphenylphosphino)propane) in the activation process. $E(C_6F_5)_3$ (E = B, Al) reacts with the pre-catalysts $[MCl_2(L)]$ under abstraction of the two chloride atoms followed by the formation of highly active "naked" Pd^{2+} through a ligand redistribution of the unstable $[Pd(dppe)]^{2+}$ cation to yield $[Pd(dppe)_2]^{2+}$ and Pd^{2+}.[16]

^1H-NMR and ^{19}F-NMR showed that the polynorbornene obtained in the presence of ethylene with activator-free $(\eta^6\text{-}C_6H_5CH_3)Ni(C_6F_5)_2$ had the end-groups –CH=CH_2 and –C_6F_5.[17] The reaction of *trans*-$[Pd(C_6F_5)Br(AsRfPh_2)_2]$ (R_f 3,5-dichloro-2,4,6-trifluorophenyl,$C_6Cl_2F_3$) and $[Pd(C_6F_5)(NCMe)(bipy)]BF_4$ with an excess of norbornene but no cocatalyst was monitored by ^{19}F-NMR and signals from (NB)C–C_6F_5 indicated that the polymerization process starts with the insertion of NB into the Pd–C_6F_5 bond.[18,19] From the cationic complex *trans*-$[Pd(C_6F_5)(AsRfPh_2)_2(NCMe)]BF_4$ and norbornene (NB : Pd = 10 : 1), the polymerization starts with the substitution of an $AsRfPh_2$ ligand *cis* to the C_6F_5 group followed by insertion of norbornene into the Pd–C_6F_5 bond and the chain growth (by ^1H-NMR and ^{19}F-NMR).[18]

Here the palladium(II) complexes **1–5** (Scheme 2) with different *N*,*N*-chelate ligands and the C_6F_5 group in combination with either the chloro- or hydroxo-substituent were used for the vinyl-homopolymerization of norbornene with MAO as activator. Complex **5** was fully characterized by 1D- and 2D-NMR spectroscopy and NMR experiments were performed with the MAO-activated catalyst **5**.

Results and discussion

Molecular structures

Compounds **1–5** are molecular palladium(II) complexes with a bidentate chelating aliphatic amine or bipyridine ligand,

Table 1 Selected bond lengths (Å) and angles (°) for **1**, **3** and **5**

Compound	**1**	**3**	**5**
Pd–C–1[a]	1.995(4)	2.010(2)	1.996(3)
Pd–N *trans* to C[b]	2.122(3)	2.0768(18)	2.121(2)
Pd–N *trans* to Cl[c]	2.081(3)	2.0368(17)	2.029(2)
Pd–Cl	2.302(1)	2.2757(5)	2.2963(6)
C-1–Pd–N-*trans*	178.48(14)	176.31(8)	169.59(10)
C-1–Pd–N-*cis*	93.14(14)	97.74(8)	91.12(10)
N–Pd–N	85.35(12)	79.93(7)	85.66(8)
C-1–Pd–Cl	88.24(11)	87.56(6)	90.08(8)
cis-N–Pd–Cl	93.27(9)	94.78(5)	93.37(6)
trans-N–Pd–Cl	178.62(9)	174.70(5)	178.31(6)
Dihedral angle $C_6(F_5)$–$PdClC_{ipso}NN$	87.9(1)	68.81(5)	57.47(6)

[a] C(arbon)1 (= C_{ipso} of C_6F_5 group) is labeled as C-1 to avoid being misread as Cl(chlorine). [b] N1 in compounds **1** and **3**, N2 in **5**. [c] N2 in compounds **1** and **3**, N4 in **5**.

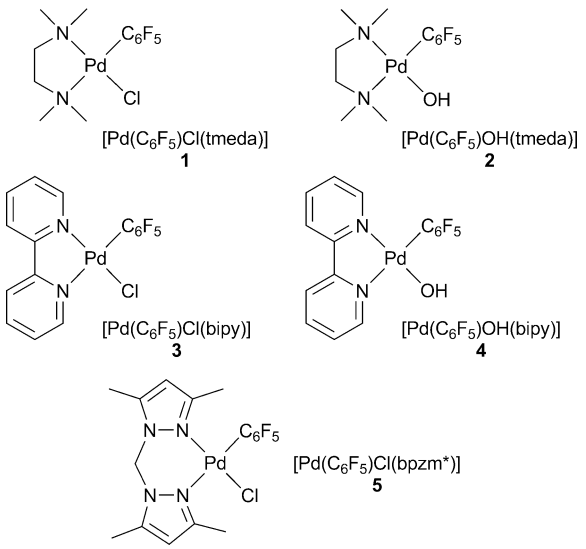

Scheme 2 Palladium(II)-C_6F_5 pre-catalysts for the vinyl polymerization of norbornene.

a pentafluorophenyl and a hydroxo or chloro ligand. The solid-state molecular structures of **1**, **3** and **5** with their slightly, chelate-induced distorted square-planar palladium coordination are depicted in Fig. 1–3, respectively. Distances and angles (Table 1) are as expected from a comparison to the related complexes $[Pd(C_6F_5)(maleimidate)(tmeda)]$,[20] $[Pd(C_6F_5)(CO_2Me)(tmeda)]$, $[Pd(C_6F_5)(SC(OMe)NPh)(tmeda)]$, $[\{Pd(C_6F_5)(4,4'\text{-}Me_2\text{-}2,2'\text{-}bipy)\}_2(\mu\text{-}CO_3)]$,[21] and $[Pd(C_6F_5)(1\text{-}Mecyt)(bpzm^*)]ClO_4$.[22]

The differences in Pd–N distances, with *trans*-N–Pd–carbon longer than *trans*-N–Pd–chlorine in **1**, **3** and **5** are in agreement with the higher *trans* influence of the C_6F_5 group, *i.e.* better σ-donor character compared to chlorine. While the solid-state structures of **3** and **5** show dihedral angles of less than 70° for the C_6F_5 ring with the $PdCl(C_{ipso})NN$ coordination plane, the most stable conformation in solution has the aryl ring roughly perpendicular to this coordination plane.[23]

Complex **1** crystallizes in the non-centrosymmetric space group *Aba*2 (now called *Aea*2).[24] In the crystal the molecules of **1** are all oriented with the tmeda side or C_6F_5 and Cl side, respectively, in

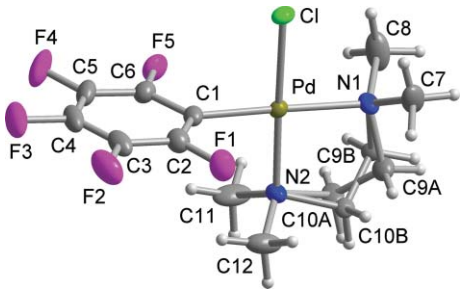

Fig. 1 Thermal ellipsoid plot (50% probability) of complex **1**, also showing the conformational racemic λ/δ disorder of the tmeda chelate ring. Selected distances and angles in Table 1.

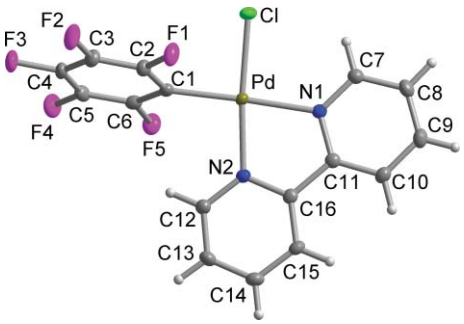

Fig. 2 Thermal ellipsoid plot (50% probability) of complex **3**. Selected distances and angles in Table 1.

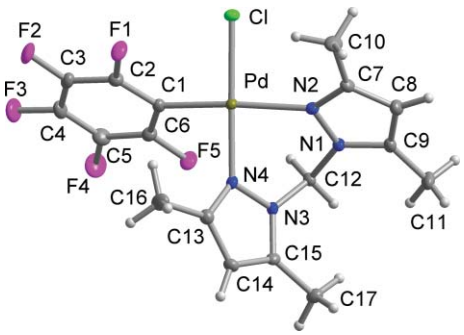

Fig. 3 Thermal ellipsoid plot (50% probability) of complex **5**. Selected distances and angles in Table 1.

the same direction along the polar *c* axis (Fig. S1 in ESI†). This polar packing[25] in the crystal of **1** occurs in domains with opposite molecular orientations so that overall the crystal is a racemic mixture. Packing diagrams for **1–3** together with supramolecular π-,[26] C–H···F/Cl-[27] and C–F···π-interactions are given in the ESI (Fig. S1–S3).†

NMR spectroscopy

An NMR study of **5** was carried out to assess the solution structure in terms of ligand fluxionality. Understanding, for example, the C_6F_5 ring rotation is important for the interpretation of the reactivity and selectivity in catalysis.[13] The ^{1}H-NMR spectrum of complex **5** (Fig. 4) was unequivocally assigned by 2D and NOE techniques.

The ^{1}H,^{1}H-TOCSY experiment (Fig. 5) allows correlations *via* small homonuclear couplings and proves that the olefinic proton with the chemical shift of $\delta = 5.80$ ppm and the methyl groups at

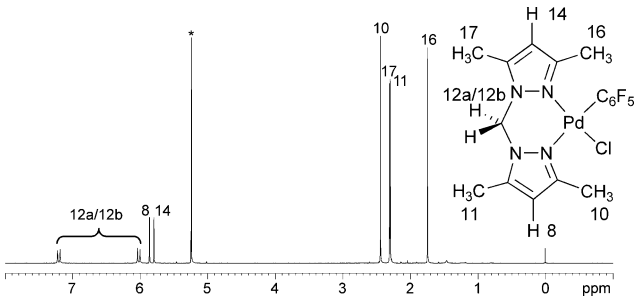

Fig. 4 ^{1}H-NMR spectrum of complex **5** in CD_2Cl_2 (0.03 mol l^{-1}) at room temperature (*$CDHCl_2$). The peak assignment is based on the ^{1}H,^{1}H-TOCSY spectrum (Fig. 5), NOE difference spectra (Fig. 6(b) and 6(c)) and the ^{1}H,^{19}F-HOESY spectrum (Fig. S16 in ESI†).

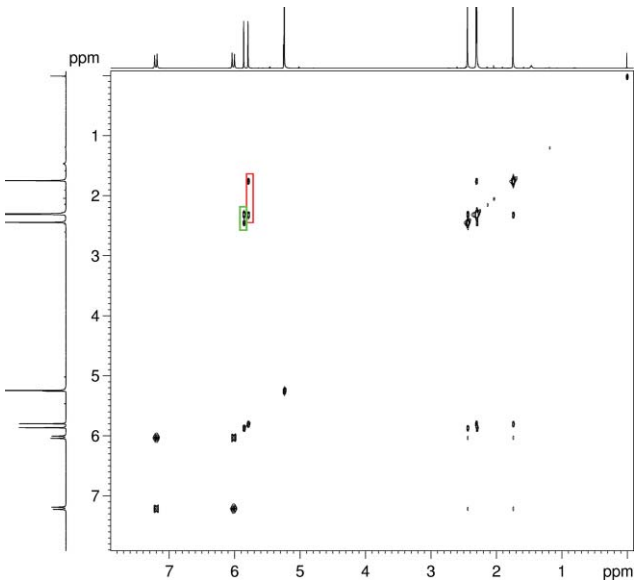

Fig. 5 ^{1}H,^{1}H-TOCSY spectrum of **5** (mixing time: 0.2 s) in CD_2Cl_2 (0.03 mol l^{-1}) at RT. Rectangles of the same color emphasize the small homonuclear coupling correlation of protons situated on the same pyrazolyl ring.

1.75 and 2.31 ppm belong to the same pyrazole ring, likewise the olefinic proton at $\delta = 5.87$ ppm and the methyl groups at 2.30 and 2.44 ppm.

In the 1D-NOE difference spectra (Fig. 6) the positions of the CH_3 groups on the pyrazolyl rings can be identified. If the methylene proton signal with the chemical shift of $\delta = 7.21$ ppm is selectively irradiated, positive NOEs are found for the resonances of the methyl groups at 2.30 and 2.31 ppm (Fig. 6(b)), which proves that these methyl groups are directed to the side of the methylene protons, whereas the methyl groups with the chemical shifts of $\delta =$ 1.75 ppm and $\delta = 2.44$ ppm point into the direction of the other ligands. The strong negative signal at $\delta = 6.02$ ppm results from chemical exchange of the methylene-bridge protons (see below). The 1D-NOE difference experiment in Fig. 6(c) was used as a duplicate test. Irradiation of the methyl group with the chemical shift of $\delta = 1.75$ did not cause a positive NOE of the methylene protons at 6.02 and 7.21 ppm, which confirms the large spatial distance between this methyl group and the methylene protons.

So far, the question is still open, which pyrazolyl ring of the bis(pyrazolyl) ligand is neighboring the pentafluorophenyl and

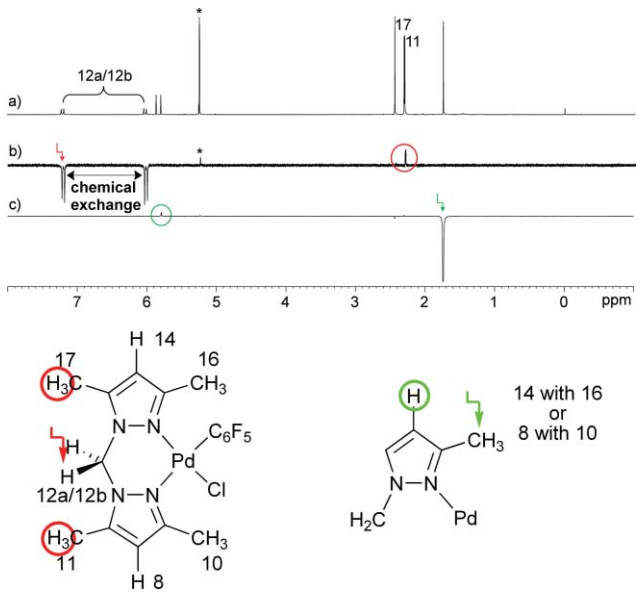

Fig. 6 (a) ^{1}H-NMR spectrum of complex **5** in CD_2Cl_2 (0.03 mol l^{-1}) at room temperature; (b) 1D-NOE difference spectrum (mixing time: 1.0 s) with signal irradiation at 7.21 ppm (*$CDHCl_2$); the positive NOE (red circle) indicates the spatial proximity; the strong negative signal at 6.02 ppm a chemical exchange – see text; (c) NOE difference spectrum (mixing time: 1.0 s) with signal irradiation at 1.75 ppm; the positive NOE (green circle) confirms the ^{1}H,^{1}H-TOCSY result that the methyl group at 1.75 and the olefinic proton at 5.80 ppm are situated on the same pyrazolyl ring.

the chlorine substituent, respectively. The answer is found in the ^{1}H,^{19}F-HOESY spectrum (Fig. S16 in ESI†). Only the methyl resonance at 1.75 ppm shows NOE cross peaks to the *ortho*-fluorine signals at –119.3 and –121.4 ppm and must therefore belong to the methyl group in the neighborhood of the C_6F_5 group. This is in good agreement with the highfield shift that is observed for this methyl resonance in comparison with the other methyl signals, because nuclei that are positioned above the plane of a phenyl ring experience a shielding effect.

By this means all proton signals are unambiguously assigned as recorded in Table 2.

The corresponding ^{13}C shifts (Table 2) are derived by the ^1J cross peaks from the ^{13}C,^{1}H-HMBC spectrum (Fig. 7). The ^1J cross peaks are distinguished from long-range correlations by their large splitting due to the large ^1J coupling constants. The quaternary carbon resonances are identified by the ^2J, ^3J and ^4J long range correlations in the same spectrum. The olefinic CH resonance at 5.80 ppm shows two ^2J cross peaks to the ^{13}C signals at 141.3 and 152.6 ppm, which therefore belong to the same pyrazolyl ring as this CH group. These two ^{13}C signals can be distinguished by the ^2J correlations from the attached methyl groups, which show that the resonance at 152.6 ppm belongs to the carbon atom attached to the methyl group with the proton resonance at 1.75 ppm. Whereas the signal at 141.3 ppm belongs to the carbon atom that is bound to the methyl group with the proton shift at 2.31 ppm. Analogously, the resonance at 140.6 ppm belongs to the carbon atom attached to the methyl group with the proton resonance at 2.30 ppm and the signal at 153.2 ppm can be attributed to the carbon atom bound to the methyl group with the proton resonance of 2.44 ppm. The methylene bridge proton signals (6.02 and 7.21 ppm) show ^1J cross

Table 2 ^{1}H- and ^{13}C-NMR assignment of the bpzm* ligand in **5**[a]

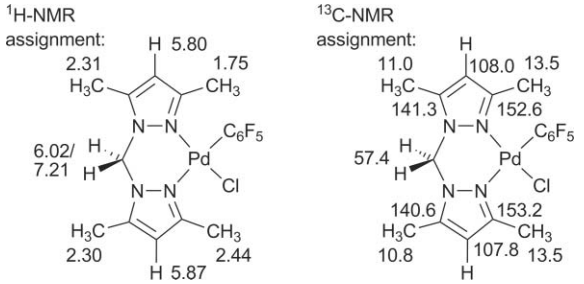

^{1}H[b]	δ (ppm)	^{13}C[b]	δ (ppm)
C16–H_3	1.75	C11	10.8
C11–H_3	2.30	C17	11.0
C17–H_3	2.31	C16	13.5
C10–H_3	2.44	C10	13.5
C14–H	5.80	C12	57.4
C8–H	5.87	C8	107.8
C12–H_2a/b	6.02	C14	108.0
C12–H_2b/a	7.21	C9	140.6
		C15	141.3
		C13	152.6
		C7	153.2

[a] Based on the ^{1}H-NMR spectrum (Fig. 4), ^{1}H,^{1}H-TOCSY (Fig. 5), NOE difference spectra (Fig. 6b, c), ^{1}H,^{19}F-HOESY (Fig. S16 in ESI†) and ^{13}C,^{1}H-HMBC spectrum (Fig. 7). [b] The ^{1}H and ^{13}C atom numbering follows the X-ray structure atom numbering in Fig. 3.

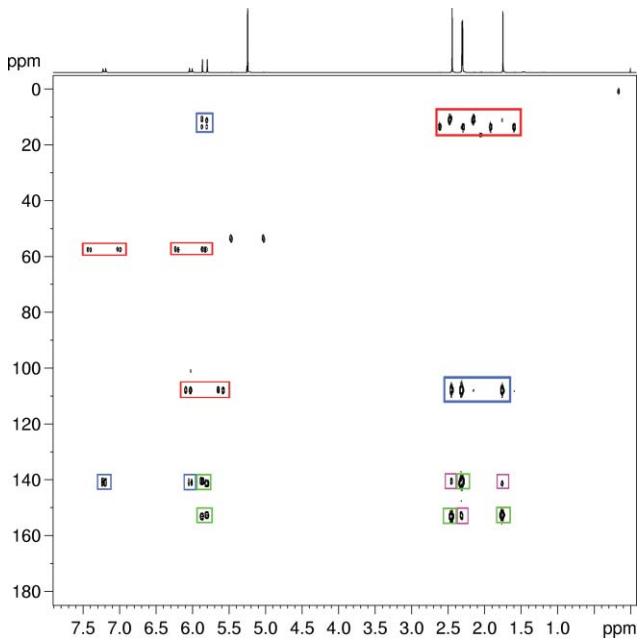

Fig. 7 ^{13}C,^{1}H-HMBC spectrum of complex **5** in CD_2Cl_2 (0.03 mol l^{-1}) at room temperature. The cross peaks represent the coupling constants $^1J(^1H,^{13}C)$ in red rectangles, $^2J(^1H,^{13}C)$ in green rectangles, $^3J(^1H,^{13}C)$ in blue rectangles and $^4J(^1H,^{13}C)$ in violet rectangles. Due to low sample concentration a good quality ^{13}C-NMR spectrum could not be measured separately (see enlarged and more detailed Fig. S4 in ESI†).

peaks to the same ^{13}C resonance in the aliphatic region at 57.4 ppm (see enlarged and more detailed Fig. S4 in ESI†).

The ^{19}F-NMR spectrum of **5** shows five signals for the C_6F_5 ligand (Fig. 8, Table 3). The signals at –119.3 and –121.4 ppm can

Table 3 ^{19}F-NMR and ^{13}C-NMR assignment for the C_6F_5 ligand in **5**

Atom[a]	^{19}F δ (ppm)	^{13}C δ (ppm)
o-F5–C6	−119.3/−121.4[b]	148.3/146.8[b]
o-F1–C2		
p-F3–C4	−161.7	137.7
m-F4–C5	−164.5/−165.0[b]	135.6/135.1[b]
m-F2–C3		
ipso-C–1		106.0

[a] The F and C atom numbering follows the X-ray structure atom numbering in Fig. 3. [b] A more specific assignment in the *ortho* and *meta* region to the individual atoms was not possible.

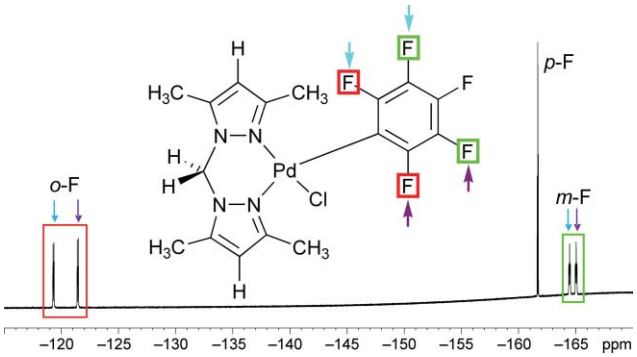

Fig. 8 ^{19}F-NMR spectrum of **5** in CD_2Cl_2 (0.03 mol l^{-1}) at RT. Identically colored arrows indicate which *o*- and *m*-F are neighbors from the cross peaks of a ^{19}F,^{19}F-COSY experiment (see Fig. S5 in ESI†).

be attributed to the *ortho*-fluorine atoms, the signal at −161.7 ppm to the *para*-fluorine atom and the signals at −164.5 and −165.0 ppm represent the *meta*-fluorine atoms of the C_6F_5 ligand because of their chemical shifts.[13] This assignment is confirmed by the ^{19}F,^{19}F-COSY spectrum (Fig. S5 in ESI†), where the signals at −119.3 ppm and −121.4 ppm in contrast to the other resonances show only one intensive cross peak. Based on this cross peak, the *meta*-F atom with the resonance at −164.5 ppm is identified as the neighbor of the *ortho*-F atom at −119.3 ppm and the *meta*-F atom at −165.0 ppm is the neighbor of the *ortho*-F atom at −121.4 ppm. This interpretation is possible because the absolute value of the $^3J(^{19}F,^{19}F)$ coupling constant is dominating the $^5J(^{19}F,^{19}F)$ coupling constant (see Table S1 in ESI†), so that the corresponding cross peaks of the ^{19}F,^{19}F-COSY spectrum display significantly different intensities.

The chemical shifts of the carbon atoms (Table 3) of the pentafluorophenyl substituent were identified by a ^{19}F,^{13}C-HSQC spectrum (see Fig. S6 in ESI†). However, the spatial positions of the different *ortho*-fluorine and *meta*-fluorine atoms were not identified. The remaining quaternary *ipso*-carbon atom was determined by a ^{19}F-decoupled ^{13}C-NMR experiment (see Fig. S7 in ESI†).

The presence of five signals in the ^{19}F-NMR spectrum of **5** (Fig. 8, see Fig. S8 for ^{19}F-NMR of **5** in acetone-d_6 in ESI†) indicates the absence of fast rotation of the C_6F_5 substituent around the M–C_{ipso} bond together with the inequivalence of the two hemi-spaces above and below the coordination plane determined by the other ligands for a near perpendicular position of the C_6F_5 ring to this plane.[13] The hindered rotation of the C_6F_5 group in **5** becomes understandable with a space-filling drawing of the structure (Fig. 9). The methyl group in the 3-position of the *cis*-positioned pyrazolyl ring blocks the rotation of the C_6F_5 ring.

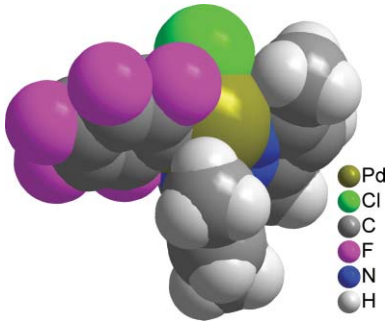

Fig. 9 Space-filling representation of complex **5** to illustrate the hindered rotation of the C_6F_5 group around the Pd–C_{ipso} bond. The C_6F_5 plane is tilted to the PdCl(C_{ipso})NN coordination plane in the solid state (interplanar angle 57.47(6)°).

The ^{19}F,^{19}F-EXSY spectrum (Fig. S9 in ESI†), however, displays cross peaks between the two *ortho*-F resonances, as well as between the two *meta*-F resonances. The cross peaks are in phase with the diagonal peaks, which indicates that they result from chemical exchange.

This exchange could be explained by a very slow rotation (slower than the NMR time scale) of the pentafluorophenyl ring or a slow flip with an exchange of the hemi-spaces. At the same time there is a chemical exchange between the methylene bridge protons of the bpzm* ligand observed in the 1D-NOE difference spectrum (Fig. 6(b)) and confirmed by a 2D ^{1}H,^{1}H-NOESY experiment (Fig. S10 in ESI†). The cross peaks between the resonances of the two methylene protons are in phase with the diagonal peaks, which again indicates that they result from chemical exchange due to a slow fluxional process. For this exchange, the following mechanism seems to be the most reasonable: a slow boat-to-boat inversion (Scheme 3) of the Pd-bpzm* chelate ring is typical for this type of complexes.[28] There is a concerted flip of the pentafluorophenyl group as a consequence of such a boat-to-boat inversion, which causes a simultaneous exchange of the chemical environment of the fluorine atoms and the methylene protons (Fig. 10). Given the fact, that almost no line broadening is observed in the line shape of the *ortho*- and *meta*-fluorine resonances at room temperature, this process has to be slow (or "frozen")[13] on the NMR timescale.

The finding of a slow ("frozen") boat-to-boat inversion and hindered C_6F_5 ring rotation in **5** (in CD_2Cl_2) contrasts with the previous interpretations (observations) in the cationic complex [Pd(C_6F_5)(1-Mecyt)(bpzm*)]ClO_4 (in acetone-d_6, 1-Mecyt = 1-methylcytosine)[22] and in the neutral complexes [Pd(C_6F_5)(CO_2R)(bpzm*)] (R = Me, Et, ^{i}Pr) (in $CDCl_3$).[21] There, the boat-to-boat inversion was also frozen (two doublets for the two diastereotopic methylene protons Ha, Hb) but the C_6F_5 ring "rotation" noted as "unhindered" (because of only three ^{19}F resonances). In Pd(C_6F_5)(CO_2R)(bpzm*)] the *o*-F resonance was broad.[21]

To quote from ref. 13: "It is very unlikely that C_6F_5 rings flanked in square-planar complexes with donor atoms of the size of chlorine or bigger are "freely rotating" and if rotation is clearly observed, a dissociative mechanism should be taken into account". In complexes [Pd(C_6F_5)X($SPPy_2Ph$)] (X = Cl, Br, I) the

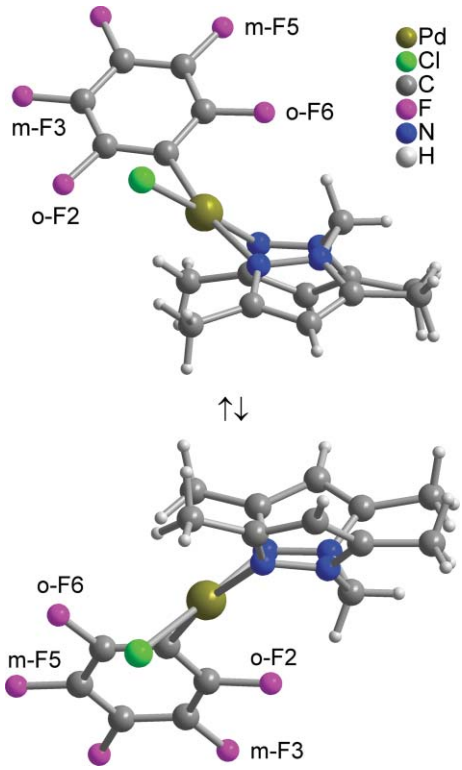

Fig. 10 Inversion-symmetry (1 − *x*, 1 − *y*, 1 − *z*) related molecules of **5** based on the boat-to-boat inversion of the chelate ring which also induces a concerted flip of C_6F_5 ring plane so that the *ortho*- and *meta*-F atoms, respectively (arbitrarily labeled as 2–6) exchange their positions without a ring rotation.

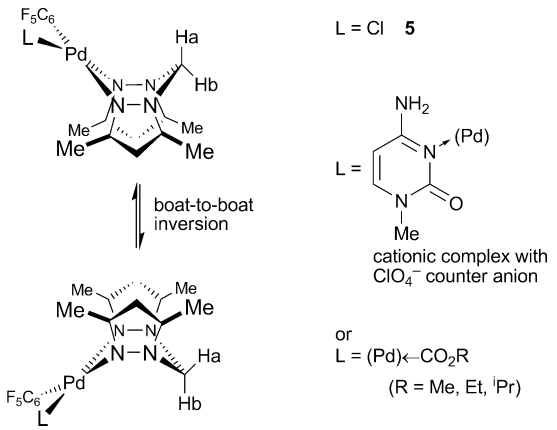

Scheme 3 Boat-to-boat inversion of the bpzm* ligand in $[Pd(C_6F_5)L(bpzm^*)]$ complexes, like **5**, $[Pd(C_6F_5)(1\text{-Mecyt})(bpzm^*)]ClO_4$ or $[Pd(C_6F_5)(CO_2R)(bpzm^*)]$ (R = Me, Et, ^{i}Pr).[21,22]

aryl rotation is very slow in $CDCl_3$ but very fast in polar solvents such acetone, suggesting that halide dissociation takes place with the energy compensated by ion solvation.[29] Thus, we propose a dissociative mechanism for the C_6F_5 ring rotation in $[Pd(C_6F_5)(1\text{-Mecyt})(bpzm^*)]ClO_4$ and $[Pd(C_6F_5)(CO_2R)(bpzm^*)]$ (R = Me, Et, ^{i}Pr), in view of the steric situation in a square-planar complex with the $Pd(C_6F_5)(bpzm^*)$ moiety, where the methyl group of the bpzm* ligand blocks the C_6F_5 ring rotation.

The ^{19}F-NMR spectra of both **1** and **3** exhibit three signals for $2F_o : 1F_p : 2F_m$ of the C_6F_5 ligand (Fig. S11 and S12 in ESI†). The related complexes $[Pd(C_6F_5)(1\text{-Mecyt})(tmeda)]ClO_4$ (in acetone-d_6),[22] $[Pd(C_6F_5)(CO_2Me)(NN)]$[21] and $[Pd(C_6F_5)(imidate)(NN)]$[20] (NN = 2,2′-bipy and tmeda) (in $CDCl_3$) also exhibit three resonances (in the ratio 2 : 1 : 2) for the *o*-, *p*- and *m*-fluorine atoms, respectively. However, $[Pd(C_6F_5)(1\text{-Mecyt})(bipy)]ClO_4$ (in DMSO-d_6) shows a hindered rotation of the C_6F_5 ring with two separate signals observed each for the *o*- and *m*-F-atoms.[22] In accordance with the space-filling diagrams of the X-ray structures of **1** and **3** (Fig. 11, 12) we argue that a free rotation of the C_6F_5 group is not necessary to yield only three resonances. An apparent symmetry plane coinciding with the coordination plane of the complex as in **1** and **3** will produce the same effect as a rotation in the spectra.[30–32] If the hemi-spaces above and below the coordination plane, which is set by the other ligands, are equivalent, so will the *o*- and *m*-F-atoms.[13] Or a dissociative mechanism: cytosine and methylcytosine (1-Mecyt) ligands on the other hand are known to easily dissociate in Pt and Pd complexes where free cytosine (in acetone-d_6) and an intermolecular exchange of cytosine between two molecules (in methanol-d_4) could by observed by NMR.[33] Otherwise, the unsymmetrical 1-Mecyt ligand will render the hemi-spaces inequivalent for the C_6F_5 group if such a dissociation does not occur.

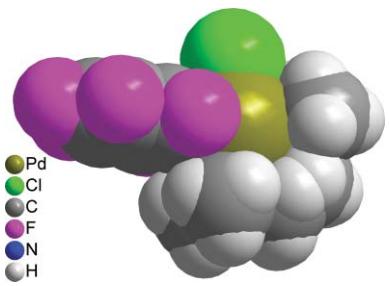

Fig. 11 Space-filling representation of complex **1**. The conformational racemic λ/δ disorder of the tmeda chelate ring creates a pseudo-mirror planes which passes through the C_6F_5 ring and renders the two *ortho*- and *meta*-F positions, respectively, equivalent even if the rotation is blocked by the tmeda methyl groups. Already in the solid state he C_6F_5 ring plane is almost perpendicular to the $PdCl(C_{ipso})NN$ coordination plane (interplanar angle 87.9(1)°).

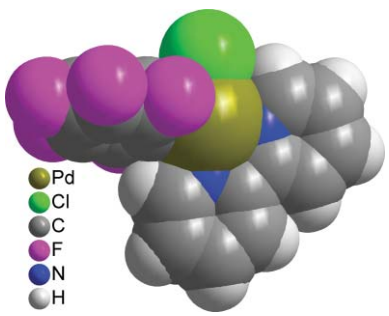

Fig. 12 Space-filling representation of complex **3**. The C_6F_5 plane is tilted to the $PdCl(C_{ipso})NN$ coordination plane in the solid state (interplanar angle 68.81(5)°). However, a perpendicular orientation is feasible in solution which then renders the two *ortho*- and *meta*-F positions, respectively, equivalent in view of the identical hemi-spaces. A full rotation may still be blocked by the C–H groups of the bipy ligand.

Table 4 Results of the NB polymerization with **1–5**/MAO

Catalyst	Time/sec	Polymer yield/g	Conversion (%)	Activity (g_{PNB}/mol_{Pd} h)
1/MAO	30	0.31	31	3.51×10^6
1/MAO	60	0.44	44	2.46×10^6
2/MAO	30	0.34	34	3.79×10^6
2/MAO	60	0.47	47	2.66×10^6
3/MAO	30	0.13	13	1.48×10^6
3/MAO	60	0.16	16	8.78×10^5
4/MAO	30	0.15	15	1.70×10^6
4/MAO	60	0.16	16	9.08×10^5
5/MAO	30	0.10	10	1.14×10^6
5/MAO	60	0.13	13	7.36×10^5

Conditions: room temperature, toluene–CH_2Cl_2 solution, total volume 10.0 mL, 1.0 g (10.6 mmol) of NB, 10.6 μmol Pd complex, molar ratio Pd : NB = 1 : 1000, Pd : Al = 1 : 100.

Norbornene polymerization

The results of the vinyl homopolymerization of NB with the pre-catalysts **1–5** are summarized in Table 4 and Fig. 13 and 14. Reaction times of 30 or 60 s were chosen intentionally. The polymerization was stopped after this time by the addition of MeOH/HCl. Such short reaction times with conversions still below 50% allow for a better differentiation or comparison of catalyst activities. The catalysts are longer living. Yet, the reaction mixture becomes more viscous with time and concomitant monomer conversion which leads to a lower reaction rate through the decrease of the diffusion rate of NB monomer to the active center. The NB polymerization is truly homogeneous only at the very beginning. With PNB formation the active complex becomes more and more embedded in the polymer matrix which represents a transfer to a heterogeneous phase, that is, a heterogeneous active complex form, and this leads to a diffusion-controlled reaction.[34] The reaction rate is then controlled by the rate of diffusion of the monomer through the polymer matrix to the enclosed active center and can no longer be compared in terms of steric or electronic ligand effects, for example. In a diffusion-controlled regime all catalysts with a faster, albeit still different insertion rate, will show the same activity due to the more rapid monomer insertion over diffusion under these conditions. In order to obtain meaningful different catalytic activities the polymerization conditions have to be chosen such as to avoid a diffusion-controlled process. Therefore, we ensured short reaction times with monomer conversions of less than 50%.[34]

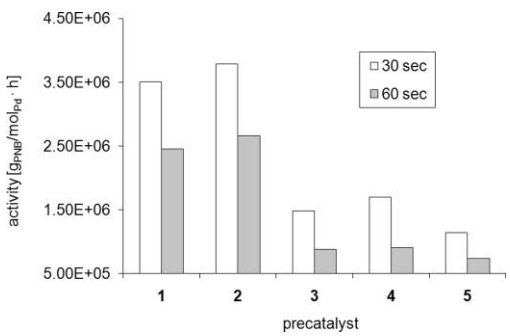

Fig. 13 Polymerization activities of MAO activated pre-catalysts **1–5** for different reaction times.

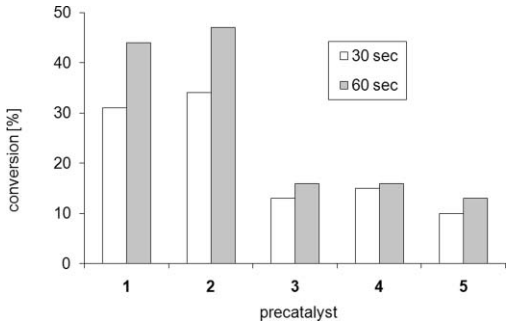

Fig. 14 Norbornene monomer conversions with **1–5**/MAO for different polymerization times.

The polymerization activities differ over a range from 7.36×10^5 g_{PNB}/mol_{Pd} h (**5**/MAO) to 3.79×10^6 g_{PNB}/mol_{Pd} h (**2**/MAO).[1,2] As expected, the activities obtained after a polymerization time of 30 s are higher than the activities for a time of 60 s (Fig. 13) while polymer yields or conversions increased with longer reaction times (Fig. 14).

The palladium complexes **1** and **2** with the aliphatic *N*,*N*-chelating *N*,*N*,*N*′,*N*′-tetramethylethylenediamine ligand showed markedly higher activities than compounds **3–5** with aromatic *N*,*N*-chelating ligands. For **1**/MAO and **2**/MAO the monomer conversions exceeded 40% within one minute of reaction time, whereas the catalytic systems **3–5**/MAO produced PNB in a range of 13 to 16% monomer conversion under the same conditions (Fig. 14). This must be attributed to the electronic effects of the aromatic substituents since the steric demand for **3** and **4** is not seen as higher than those of **1** and **2**. In the literature electron-withdrawing ligands or substituents are usually viewed as activity enhancing in complexes activated for NB polymerization.[35–42] Aromatic nitrogen ligands are stronger and electron-withdrawing ligands in the spectrochemical series than aliphatic amine ligands due to their modest π-accepting character whereas aliphatic amines are pure σ-donor ligands. Hence, our activity order is counterintuitive. Therefore, we argue here with a kinetic activation effect. Previous work has shown that upon borane or MAO activation all ligands can be lost to give a "naked" Pd^{2+} as the active species.[16] Hence, more weakly bound ligands which will be removed faster will lead more quickly to the active palladium dications. Based on dissociation energies for M^+–L (L = NH_3, pyridine) the aliphatic diamine ligands are bound more weakly to a metal atom than the aromatic pyridine ligands by about 20 kJ mol^{-1}.[43] We are not aware of any similar comparison between aliphatic and aromatic dinitrogen ligands. There is no significant effect of the chloro *vs.* hydroxo ligand on the polymerization activity as shown by a comparison of catalysts **1**/MAO *vs.* **2**/MAO and **3**/MAO *vs.* **4**/MAO. Complexes with the hydroxo ligands appear to be, if any, only very slightly more active. The often encountered insolubility of the obtained PNBs made a further characterization of the polymer molar mass and mass distribution by gel permeation chromatography impossible.[1,2,3]

^{19}F solid-state NMR-experiments were attempted with the PNBs obtained by the catalytic systems **1–5**/MAO to try to get information on the polymer start group, for a better understanding of the mechanism of the norbornene polymerization, whose initiation step is of high interest. However, no signals in the ^{19}F-spectra could be detected. This could be attributed to the fact,

that the PNBs were of too high molecular weight to determine the end-group by NMR or that the C_6F_5 ligand is not the start group, that is, the first insertion does not occur into the Pd–C_6F_5 bond (see below).

Pre-catalyst activation

Complex **5** was chosen for an NMR study to elucidate the activation mechanism with MAO at two different molecular Pd : Al ratios of 1 : 10 and 1 : 100. At a Pd : Al ratio of 1 : 10 the ^{1}H-NMR spectrum is dominated by the signals of the unchanged complex **5**, which are slightly shifted compared to the resonances of pure **5** mainly due to the different solvent (toluene-d_8 *versus* CD_2Cl_2). In addition, less intense resonances are found for a complete second set of signals of the bpzm* ligand (Fig. 15(a)). At 0.43 ppm another resonance appears with an integral identical to the integrals of the CH_3 groups of this second bpzm* set. If this signal is selectively irradiated, a positive NOE is found for the methyl group on the bis(3,5-dimethylpyrazol-1-yl)methane ligand with the chemical shift $\delta = 2.18$ ppm (Fig. 15(b)).

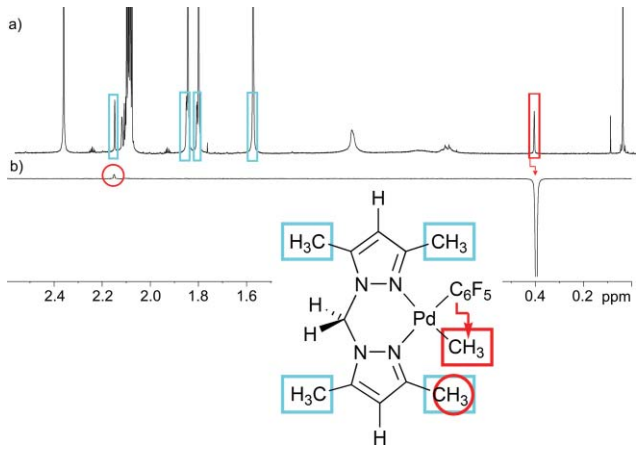

Fig. 15 (a) Methyl region of the ^{1}H-NMR spectrum of the MAO activated complex **5** with a molecular Pd : Al ratio of 1 : 10 (in a 1 : 1 mixture of CD_2Cl_2 and toluene-d_8 as a 0.03 mol l^{-1} solution in Pd, RT). Cyan rectangles highlight the newly formed bpzm* signal set, the red rectangle the new methyl resonance. There is signal overlap at 1.60 ppm for **5** and its methylated form [Pd(C_6F_5)CH_3(bpzm*)]. (b) 1D NOE-difference spectrum of **5**/MAO with signal irradiation at 0.43 ppm and the positive NOE (red circle).

In a ^{13}C,^{1}H-correlation (Fig. S13 in ESI†) the resonance of the corresponding C atom is identified at –13 ppm. This strongly suggests that the new resonance at 0.43 ppm belongs to a CH_3 group directly bound to a Pd atom that is still coordinated by a bpzm* ligand. This Pd–CH_3 group is then neighboring the CH_3 group of the pyrazolyl ring with the proton resonance at 2.18 ppm. The fact, that one pyrazolyl methyl group of the new set is still upfield shifted (1.60 ppm) as in **5** (1.75 ppm) leads to the conclusion that the C_6F_5 substituent remained bound to Pd and it is the chlorine which is replaced by the entering methyl group. According to the proton integrals the ratio between the methylated complex and complex **5** is 1 : 6.7, amounting to 13% chlorine-to-methyl exchange (see Fig. S14 with integrals in ESI†).

Consistent with the proton NMR, the ^{19}F-NMR spectrum also shows the signals of **5** and the resonances of a second pentafluorophenyl group still bound to a palladium atom (Fig. 16(b) and enlarged version in Fig. S15(a),(b) in ESI†). The integrals of the fluorine resonances provide the same ratio of 1 : 6.7 (new complex to **5**) as the integrals in the ^{1}H-NMR spectrum. There is, however, only one signal, each, of the *ortho*- and *meta*-F atoms of the C_6F_5 ligand in the methylated complex, albeit significantly broadened.

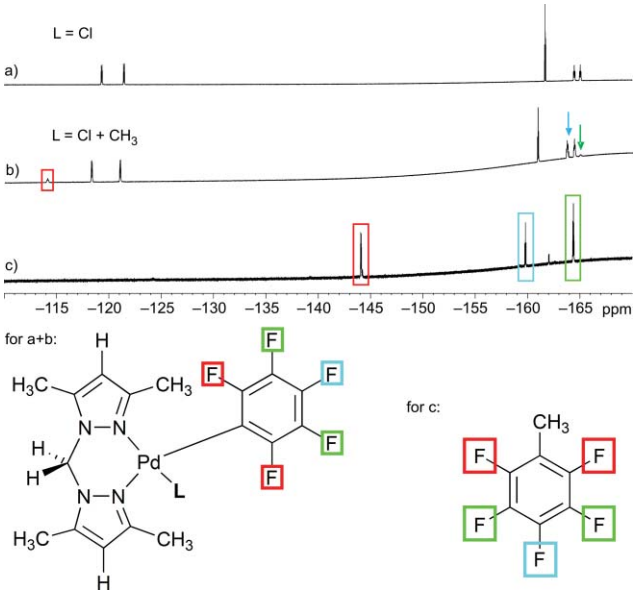

Fig. 16 (a) ^{19}F-NMR spectrum of the unactivated complex **5** in CD_2Cl_2 (L = Cl) (0.03 mol l^{-1}) at room temperature. (b) ^{19}F-NMR spectrum of **5**/MAO (L = CH_3) (molecular Pd : Al ratio of 1 : 10), see also Fig. S15(a),(b) in ESI† for an enlarged version. (c) ^{19}F-NMR spectrum of **5**/MAO (molecular Pd : Al ratio of 1 : 100).

In Table 5, the chemical shifts of the methylated complex from **5**/MAO with Pd : Al = 1 : 10 are summarized. The ^{13}C resonances are derived from the ^{13}C,^{1}H-HMBC spectrum for **5**/MAO (Fig. S13 in ESI†).

Table 5 ^{1}H-, ^{13}C- and ^{19}F-NMR assignment of the methylated complex in **5**/MAO at a molar Pd : Al ratio of 1 : 10[a]

^{1}H[b]	δ (ppm)	^{13}C[b,c]	δ (ppm)	^{19}F[b]	δ (ppm)
Pd–CH_3	0.43	Pd-CH_3	–13.0	F1,F5	114.1
C16–H_3	1.60[d]	C11	10.3	F3	163.8
C11–H_3	1.84	C17	10.6	F2,F4	165.0
C17–H_3	1.88	C16	13.6		
C10–H_3	2.18	C10	14.0		
C14–H	5.37	C12	56.8		
C8–H	5.54	C8	107.8		
C12–H_2a/b	5.32	C14	108.0		
C12–H_2b/a	6.76	C15	140.3		
		C9	141.0		
		C7	151.8		
		C13	152.7		

[a] Based on the ^{1}H-NMR spectrum (*cf.* Fig. 15(a) – full range as Fig. S14 in ESI†), ^{13}C,^{1}H-HMBC spectrum (Fig. S13 in ESI†) and the ^{19}F-NMR spectrum (Fig. 16(b)). The spectra were recorded in a 1 : 1 mixture of CD_2Cl_2 and toluene-d_8 as a 0.03 mol l^{-1} solution with respect to Pd. [b] The F and C atom numbering follows the X-ray structure atom numbering in Fig. 3. [c] An assignment of the ^{13}C resonances for C1-C6 of the C_6F_5 ligand was not undertaken. [d] There is signal overlap at 1.60 ppm for **5** and its methylated form.

A molecular Pd : Al ratio of 1 : 100 for **5**/MAO led to an immediate dark palladium metal precipitate in the NMR tube, probably due to formation of "naked" Pd^{2+} from complete ligand abstraction and subsequent reduction of reactive Pd^{2+} in the absence of the stabilizing norbornene monomer.[16] In the ^{19}F-NMR spectrum no signals of a Pd-bound pentafluorophenyl ligand could be found anymore. Instead, the resonances of the corresponding oxidation product pentafluorotoluene, C_6F_5-CH_3 were almost exclusively detected (Fig. 16(c)).

Conclusions

Complex [Pd(C_6F_5)Cl(bpzm*)], **5** was fully characterized by NMR spectroscopy in terms of complete peak assignment by various 1D and 2D ^{1}H-, ^{13}C- and ^{19}F-NMR techniques. The bpzm* boat-to-boat inversion occurs at a rate slower than the NMR time scale together with a concomitant change of the C_6F_5 atom positions (no ring rotation). The presence of only three ^{19}F NMR signals for complexes [Pd(C_6F_5)Cl(tmeda)], **1** and [Pd(C_6F_5)Cl(bipy)], **3** is interpreted as being due to the identical hemi-spaces above and below an apparent symmetry plane coinciding with the Pd-coordination plane instead of free ring rotation. X-Ray structures of **1**, **3** and **5** agree to the hindered ring rotation due to ligand repulsion. Five palladium(II) pre-catalysts with *N*,*N*-chelating ligands and chloro *vs.* hydroxo substituents could be activated with MAO towards the vinyl polymerization of NB and showed activities of more than 10^6 g_{PNB}/mol_{Pd} h. The complexes with the aliphatic *N*,*N*-chelating ligand *N*,*N*,*N*′,*N*′-tetramethylethylenediamine gave significantly higher catalytic activities than the Pd complexes bearing aromatic *N*,*N*-chelating substituents. This behavior is reasoned by faster MAO activation through a more rapid ligand abstraction of the more weakly bound aliphatic *N*,*N*-ligand together with the chloro or hydroxo ligands to give the active, almost "naked" Pd^{2+} cations. Furthermore, ^{1}H-, ^{13}C- and ^{19}F-NMR studies of the MAO activated complex **5** showed a chlorine-to-methyl exchange for a molar Pd : Al ratio of 1 : 10. At a Pd : Al ratio of 1 : 100 for **5**/MAO no Pd-bound C_6F_5 could be detected any more but only the species pentafluorotoluene, C_6F_5-CH_3. Also, an immediate formation of metallic palladium occurred.

Experimental

All work involving air-and/or moisture-sensitive compounds was carried out with standard vacuum, Schlenk, or dry-box techniques. IR spectra were recorded on a Nicolet Magna-IR 760 Spectrometer. MAO (10% solution in toluene, Witco) was used as received. Toluene and dichloromethane were dried under argon with an MBraun SPS-800 system. The drying agent for toluene was activated Al_2O_3 in addition to a copper-catalyst used as an oxygen scavenger. Al_2O_3 alone was used as the drying agent for dichloromethane. After the drying process the water content was determined by a Karl-Fischer titration, which showed a water mass of 0.0008% for toluene and 0.0004% for dichloromethane. Subsequently, the solvents were stored under argon prior to use. Norbornene (Acros) was purified by distillation under argon and used as a 7.07 mol l^{-1} solution in toluene. The palladium complexes **1** and **3**,[44] **2**, **4** and **5** were prepared as reported previously.[21]

General polymerization procedure

The palladium complexes/pre-catalysts (1.06×10^{-2} mmol) were dissolved in 4 ml of CH_2Cl_2 to give a light-yellow colored clear solution ($c_{Pd} = 2.65 \times 10^{-3}$ mmol ml^{-1}). A 25 ml Schlenk-flask was charged with the NB/toluene solution (1.5 ml, 10.6 mmol NB) and an additional 3.8 ml of toluene. Then, the MAO solution (0.7 ml) was added to reach a total reaction volume of 10 ml. After 1 min of stirring the pre-catalyst/dichloromethane solution was added *via* syringe to start the polymerization. The polymerizations were run at room temperature. The activity did not lead to a significant warming of the reaction mixture; hence, no cooling bath was necessary. After 30 or 60 s the polymerization was stopped by the addition of a methanol/concentrated HCl mixture (10 : 1, 30 ml). The precipitated polymer was filtered, washed with methanol, and dried *in vacuo* for 6 h. Each polymerization experiment was performed twice to ensure reproducibility. The vinyl type polymerization of norbornene was ensured by infrared spectroscopy of the polymers which showed no absorption bands in the region of 1640 cm^{-1}, which otherwise would indicate the presence of double bonds.

X-Ray crystallography†

A suitable single crystal of **1**, **3** or **5** was carefully selected under a polarizing microscope. Data Collection: Bruker Smart Apex diffractometer Mo Kα radiation ($\lambda = 0.71073$ Å), graphite monochromator, double-pass method ω-scan, temperature 100(2) K. Data collection with SMART,[45] cell refinement and data reduction with SAINT,[45] experimental absorption correction with SADABS.[46] Structure Analysis and Refinement: the structures were solved by direct methods (SHELXS-97); refinement was done by full-matrix least squares on F^2 using the SHELXL-97 program suite.[47] All non-hydrogen positions were refined with anisotropic displacement parameters. Hydrogen atoms were positioned geometrically and refined using riding models with $U_{iso}(H) = 1.2\ U_{eq}(CH, CH_2)$ and $U_{iso}(H) = 1.5\ U_{eq}(CH_3)$.

In the structure of **1** the ethylene moiety of the tmeda ligand was refined with equally occupied split positions for the λ and δ conformers as in the previously reported 173 K structure (Refcode MAGPIU).[24] The structure of **1** was refined in a twin-refinement with a BASF-scale factor to a near racemic twin. An attempted solution and refinement in the super-group *Cmca* (*Cmce*) did not give satisfactory results but gave two positions for each ligand around the Pd atom on the special position (0 y z). The program PLATON[48] also did not suggest a space group change but confirmed the present non-centrosymmetric space group *Aba*2 (now called *Aea*2) as in MAGPIU.[24] The three largest residual Fourier peaks (2.28, 1.96 and 0.64) are all found within 0.83 Å of the Pd atom in **1**. The deepest hole (–0.44) is 1.23 Å from the Pd atom. Crystal data and details on the structure refinement are given in Table 6. Graphics were drawn with DIAMOND,[49] analyses on the supramolecular π-, C–H···F/Cl- and C–F···π-interactions with PLATON for Windows.[48]

NMR spectroscopy

NMR spectra of **1** and **3** were measured on a Bruker 300 MHz spectrometer. The 1D and 2D-NMR experiments with **5** were performed on a Bruker Avance II 400 WB spectrometer (400 MHz

Table 6 Crystal data and structure refinement for **1**, **3** and **5**

Compound	**1** (*cf.* ref. 24)	**3**	**5**
Empirical formula	$C_{12}H_{16}ClF_5N_2Pd$	$C_{16}H_8ClF_5N_2Pd$	$C_{17}H_{16}ClF_5N_4Pd$
M/g mol^{-1}	425.12	465.09	513.19
Crystal size/mm	0.27 × 0.17 × 0.03	0.32 × 0.08 × 0.08	0.17 × 0.16 × 0.05
Crystal appearance	Plate, pale-yellow	Needle, pale-yellow	Prism, colorless
2θ range/°	4.05–56.20	3.20–56.44	3.58–54.30
h; k; l range	±16; −25, 26; ±15	±9; −21, 22; ±33	±9; −21, 22; ±19
Crystal system	Orthorhombic	Orthorhombic	Monoclinic
Space group	*Aba*2 (*Aea*2)	*Pbca*	$P2_1/c$
a/Å	12.5450(7)	7.0364(3)	7.1660(3)
b/Å	19.9097(8)	16.9602(7)	17.2246(6)
c/Å	11.9976(8)	25.4701(11)	15.2372(6)
β/°	90	90	96.7630(10)
V/Å^3	2996.6(3)	3039.6(2)	1867.66(13)
Z	8	8	4
D_c/g cm^{-3}	1.885	2.033	1.825
F(000)	1680	1808	1016
μ/mm^{-1}	1.464	1.454	1.195
Max/min transmission	0.9574/0.6933	0.8926/0.6534	0.9427/0.8227
Reflections collected	16 309	32 576	20 956
Indep. reflections	3408 (0.0558)	3596 (0.0260)	4116 (R_{int} = 0.0279)
Obs. reflect [$I > 2\sigma(I)$]	3266	3357	3846
Parameters refined	209	226	253
Max./min. $\Delta\rho$ [a]/e Å^{-3}	2.279/−0.439	0.478/−0.329	0.736/−0.705
R_1, wR_2 [$I > 2\sigma(I)$][b]	0.0326/0.0753	0.0284/0.0606	0.0293/0.0728
R_1, wR_2 (all reflect.)[b]	0.0344/0.0763	0.0257/0.0619	0.0319/0.0744
Goodness-of-fit on F^2[c]	1.081	1.114	1.067
Weight scheme w; a/b[d]	0.0493/0.0000	0.0285/3.5253	0.0356/3.4764
Flack parameter[e]	0.45(3)[f]	—	—

[a] Largest difference peak and hole. [b] $R_1 = [\sum(\|F_o| - |F_c\|)/\sum|F_o|]$; w$R_2 = [\sum[w(F_o^2 - F_c^2)^2]/\sum[w(F_o^2)^2]]^{1/2}$. [c] Goodness-of-fit = $[\sum[w(F_o^2 - F_c^2)^2]/(n-p)]^{1/2}$. [d] w = $1/[\sigma^2(F_o^2) + (aP)^2 + bP]$ where $P = (\max(F_o^2 \text{ or } 0) + 2F_c^2)/3$. [e] BASF-scale factor, absolute structure parameter.[50] [f] See comment in X-ray crystallography section.

for ^{1}H, 376.54 MHz for ^{19}F) in regular NMR tubes with a screw cap to ensure an inert atmosphere. The NMR tube was filled in a Schlenk tube under argon atmosphere. For the measurements with the pure pre-catalyst **5** (15.4 mg, 0.03 mmol) dichloromethane-d_2 (CD_2Cl_2, 1 ml) was used as the solvent. The procedure for the MAO activated complex was as follows: a 10% MAO solution in toluene (0.21 ml, 0.30 mmol Al) was placed in a Schlenk flask and the toluene was removed under reduced pressure. After complete evaporation it was replaced by toluene-d_8 (0.5 ml) to ensure a total volume of 1 ml, which is suitable for NMR measurements. For a molecular Pd : Al ratio of 1 : 10 compound **5** (15.4 mg, 0.03 mmol) was dissolved in dichloromethane-d_2 (0.5 ml), then, the MAO/toluene-d_8 solution was added. For a molecular Pd : Al ratio of 1 : 100 the procedure was the same except for use of the tenfold amount of the 10% MAO solution in toluene (2.1 ml). In this case a black precipitate appeared immediately. With total correlation spectroscopy (TOCSY[51]) coherence transfer is possible between all coupled nuclei in a spin system, even if they are not directly coupled. The TOCSY spectrum was acquired with spectral widths of 3.2 kHz in both dimensions and a 256·1k ($t_1 \cdot t_2$) data matrix collecting 8 scans for each time increment. In the 1D nuclear overhauser effect (NOE) difference spectroscopy[52] the intensity change of a certain resonance upon the irradiation of another spin can be related to the distance between the two nuclei. The spectra were detected using the DPFGSENOE experiment. The 2D nuclear or heteronuclear overhauser enhancement spectroscopy (NOESY,[53] HOESY[54]) allows to detect homonuclear or heteronuclear through-space NOE connectivities between non-bonded nuclei. The ^{1}H,^{1}H-NOESY was performed with spectral widths of 3.24 kHz in both dimensions and a 256·2k data matrix collecting 24 scans for each time increment. The ^{19}F,^{19}F-EXSY (exchange spectroscopy) was performed with spectral widths of 22.7 kHz for both dimensions collecting a 256·2k data matrix with 8 scans for each time increment. The ^{1}H,^{19}F-HOESY was detected with a spectral width of 3.0 kHz in f2 (^{19}F) and 3.2 kHz in f1 (^{1}H) using a data matrix of 256·2k and accumulating 72 scans for each time increment. The heteronuclear multiple bond correlation (HMBC[55]) allows to obtain a 2D heteronuclear chemical shift correlation map between long-range coupled ^{1}H and heteronuclei. The delay 1/(2 J) was optimized to a value of 62.5 ms (8 Hz). The spectrum was detected with a spectral width of 3.2 kHz in f2 (^{1}H) and 19.1 kHz in f1 (^{13}C) and a data matrix of 512·2k collecting 16 scans for each time increment.

Acknowledgements

This work was supported by the Ministerio de Ciencia y Tecnología (Project CTQ2008-02178/BQU), Spain.

Notes and references

1 F. Blank and C. Janiak, *Coord. Chem. Rev.*, 2009, **253**, 827–861.
2 C. Janiak, P.-G. Lassahn and V. Lozan, *Macromol. Symp.*, 2006, **236**, 88–99.

3 C. Janiak and P.-G. Lassahn, *J. Mol. Catal. A: Chem.*, 2001, **166**, 193–209.
4 Recent work: X. Meng, G.-R. Tang and G.-X. Jin, *Chem. Commun.*, 2008, 3178–3180; W.-G. Jia, Y.-B. Huang, Y.-J. Lin and G.-X. Jin, *Dalton Trans.*, 2008, 5612–5620; W. Zuo, W.-H. Sun, S. Zhang, P. Hao and A. Shiga, *J. Polym. Sci., Part A: Polym. Chem.*, 2007, **45**, 3415; J. Hou, S. Jie, W. Zhang and W.-H. Sun, *J. Appl. Polym. Sci.*, 2006, **102**, 2233.
5 B. Berchtold, V. Lozan, P.-G. Lassahn and C. Janiak, *J. Polym. Sci., Part A: Polym. Chem.*, 2002, **40**, 3604–3614.
6 N. R. Grove, P. A. Kohl, S. A. B. Allen, S. Jayaraman and R. Shick, *J. Polym. Sci., Part B: Polym. Phys.*, 1999, **37**, 3003.
7 A. Hideki, A. Satoshi, M. Hiroshi, and M. Junichi, Patent EPO445755, Equivalents DE69129600, JP4063807, Idemitsu Kosan Co. (Jpn.), 1991.
8 T. F. A. Haselwander, W. Heitz, S. A. Krügel and J. H. Wendorff, *Macromol. Chem. Phys.*, 1996, **197**, 3435; and references therein.
9 K. H. Park, R. J. Twieg, R. Ravikiran, L. F. Rhodes, R. A. Shick, D. Yankelevich and A. Knoesen, *Macromolecules*, 2004, **37**, 5163.
10 T. Hoskins, W. J. Chung, A. Agrawal, P. J. Ludovice, C. L. Henderson, L. D. Seger, L. F. Rhodes and R. A. Shick, *Macromolecules*, 2004, **37**, 4512.
11 H. Y. Cho, D. S. Hong, D. W. Jeong, Y.-D. Gong and S. I. Woo, *Macromol. Rapid Commun.*, 2004, **25**, 302; D. M. Shin, S. U. Son, B. K. Hong, Y. K. Chung and S.-H. Chun, *J. Mol. Catal. A: Chem.*, 2004, **210**, 35; H. Liang, J. Liu, X. Li and Y. Li, *Polyhedron*, 2004, **23**, 1619; X. Mi, Z. Ma, L. Wang, Y. Ke and Y. Hu, *Macromol. Chem. Phys.*, 2003, **204**, 868; A. S. Abu-Surrah, U. Thewalt and B. Rieger, *J. Organomet. Chem.*, 1999, **587**, 58–66.
12 V. Lozan, P.-G. Lassahn, C. Zhang, B. Wu, C. Janiak, G. Rheinwald and H. Lang, *Z. Naturforsch.*, 2003, **58b**, 1152–1164.
13 P. Espinet, A. C. Albéniz, J. A. Casares and J. M. Martínez-Ilarduya, *Coord. Chem. Rev.*, 2008, **252**, 2180–2208.
14 T. M. J. Anselment, S. I. Vagin and B. Rieger, *Dalton Trans.*, 2008, 4537–4548.
15 P.-G. Lassahn, V. Lozan and C. Janiak, *Dalton Trans.*, 2003, 927–935.
16 P.-G. Lassahn, V. Lozan, B. Wu, A. S. Weller and C. Janiak, *Dalton Trans.*, 2003, 4437–4450.
17 D. A. Barnes, G. M. Benedikt, B. L. Goodall, S. S. Huang, H. A. Kalamarides, S. Lenhard, L. H. McIntosh, III, K. T. Selvy, R. A. Shick and L. F. Rhodes, *Macromolecules*, 2003, **36**, 2623.
18 J. A. Casares, P. Espinet and G. Salas, *Organometallics*, 2008, **27**, 3761–3769.
19 R. López-Fernández, N. Carrera, A. C. Albéniz and P. Espinet, *Organometallics*, 2009, **28**, 4996–5001.
20 J. Ruiz, C. Vicente, N. Cutillas and J. Pérez, *Dalton Trans.*, 2005, 1999–2006.
21 J. Ruiz, M. T. Martinez, F. Florenciano, V. Rodriguez, G. López, J. Pérez, P. A. Chaloner and P. B. Hitchcock, *Inorg. Chem.*, 2003, **42**, 3650–3661.
22 J. Ruiz, N. Cutillas, C. Vicente, M. D. Villa and G. López, *Inorg. Chem.*, 2005, **44**, 7365–7376.
23 M. A. Bennett, G. B. Robertson, A. Rokicki and W. A. Wickramaringhe, *J. Am. Chem. Soc.*, 1988, **110**, 7098.
24 R. P. Hughes, A. J. Ward, J. A. Golen, C. D. Incarvito, A. L. Rheingold and L. N. Zakharov, *Dalton Trans.*, 2004, 2720–2727.
25 C. Janiak, A.-C. Chamayou, A. K. M. R. Uddin, M. Uddin, K. S. Hagen and M. Enamullah, *Dalton Trans.*, 2009, 3698–3709; Y.-T. Wang, G.-M. Tang, Y.-Q. Yong, T.-X. Qin, T.-D. Li, J.-B. Ling and X.-F. Long, *Inorg. Chem. Commun.*, 2009, **12**, 1164–1167; W.-W. Zhou, J.-T. Chen, G. Xu, M.-S. Wang, J.-P. Zou, X.-F. Long, G.-J. Wang, G.-C. Guo and J.-S. Huang, *Chem. Commun.*, 2008, 2762–2764; M. D. Stephenson and M. J. Hardie, *Dalton Trans.*, 2006, 3407–3417.
26 C. Janiak, *J. Chem. Soc., Dalton Trans.*, 2000, 3885–3896; H. W. Roesky and M. Andruh, *Coord. Chem. Rev.*, 2003, **236**, 91.
27 J. Ruiz, V. Rodríguez, C. de Haro, A. Espinosa, J. Pérez and C. Janiak, *Dalton Trans.*, 2010, **39**, 3290–3301; E. Redel, M. Fiederle and C. Janiak, *Z. Anorg. Allg. Chem.*, 2009, **635**, 1139–1147; H. A. Habib, A. Hoffmann, H. A. Höppe, G. Steinfeld and C. Janiak, *Inorg. Chem.*, 2009, **48**, 2166–2180; J. Ruiz, M. D. Villa, V. Rodríguez, N. Cutillas, C. Vicente, G. López and D. Bautista, *Inorg. Chem.*, 2007, **46**, 5448–5449; G. Althoff, J. Ruiz, V. Rodríguez, G. López, J. Pérez and C. Janiak, *CrystEngComm*, 2006, **8**, 662–665; G. R. Desiraju and T. Steiner, The weak hydrogen bond, *IUCr Monograph on Crystallography*, 1999, vol. 9, Oxford Science, Oxford.
28 S. Tsuji, D. C. Swenson and R. F. Jordan, *Organometallics*, 1999, **18**, 4758–4764.
29 J. A. Casares, S. Coco, P. Espinet and Y.-S. Lin, *Organometallics*, 1995, **14**, 3058.
30 S. Coco and P. Espinet, *J. Organomet. Chem.*, 1994, **484**, 113–118.
31 U. Armador, E. Delgado, J. Forniés, E. Hernández, E. Lalinde and M. T. Moreno, *Inorg. Chem.*, 1995, **34**, 5279–5284.
32 L. R. Falvello, J. Forniés, R. Navarro, A. Rueda and E. P. Urriolabeitia, *Organometallics*, 1996, **15**, 309–316.
33 A. Klein, T. Schurr, H. Scherer and N. S. Gupta, *Organometallics*, 2007, **26**, 230–233; K. Butsch, S. Elmas, N. S. Gupta, R. Gust, F. Heinrich, A. Klein, Y. von Mering, M. Neugebauer, I. Ott, M. Schäfer, H. Scherer and T. Schurr, *Organometallics*, 2009, **28**, 3906–3915.
34 C. Janiak, K. C. H. Lange, U. Versteeg, D. Lentz and P. H. M. Budzelaar, *Chem. Ber.*, 1996, **129**, 1517–1529.
35 X.-Q. Lu, F. Bao, B.-S. Kang, Q. Wu, H.-Q. Liu and F.-M. Zhu, *J. Organomet. Chem.*, 2006, **691**, 821.
36 N. H. Tarte, H. Y. Cho and S. I. Woo, *Macromolecules*, 2007, **40**, 8162.
37 D. H. Lee, J. Y. Lee, J. Y. Ryu, Y. Kim, C. Kim and I.-M. Lee, *Bull. Korean Chem. Soc.*, 2006, **27**, 1031–1037.
38 C. Carlini, M. Martinelli, A. M. R. Galletti and G. Sbrana, *J. Polym. Sci., Part A: Polym. Chem.*, 2006, **44**, 1514.
39 Y.-Z. Zhu, J.-Y. Liu, Y.-S. Li and Y.-J. Tong, *J. Organomet. Chem.*, 2004, **689**, 1295.
40 X. He and Q. Wu, *J. Appl. Polym. Sci.*, 2006, **101**, 4172.
41 M. Schroers, J. Demeter, K. Dehnicke and A. Greiner, *Macromol. Chem. Phys.*, 2002, **203**, 2658.
42 C. Carlini, S. Giaiacopi, F. Marchetti, C. Pinzino, A. M. R. Galletti and G. Sbrana, *Organometallics*, 2006, **25**, 3659.
43 *CRC Handbook of Chemistry and Physics*, 90th edn, CRC Press, Boca Raton, 2009–2010, p. 9–91.
44 R. Uson, J. Forniés and F. Martinez, *J. Organomet. Chem.*, 1976, **112**, 105.
45 *SMART, Data Collection Program for the CCD Area-Detector System; SAINT, Data Reduction and Frame Integration Program for the CCD Area-Detector System*, Bruker Analytical X-ray Systems, Madison, Wisconsin, USA, 1997-2006.
46 G. M. Sheldrick, *SADABS, Program for area detector adsorption correction*, Institute for Inorganic Chemistry, University of Göttingen, Germany, 1996.
47 G. M. Sheldrick, *Acta Crystallogr., Sect. A: Found. Crystallogr.*, 2008, **64**, 112–122.
48 A. L. Spek, *J. Appl. Crystallogr.*, 2003, **36**, 7; *PLATON – A Multipurpose Crystallographic Tool*, Utrecht University, Utrecht, The Netherlands; A. L. Spek, 2008, Windows implementation; L. J. Farrugia, University of Glasgow, Scotland, Version 40608, 2008.
49 K. Brandenburg, *Diamond (Version 3.2c), Crystal and Molecular Structure Visualization*, Crystal Impact, K. Brandenburg and H. Putz, Gbr, Bonn (Germany), 2009.
50 H. D. Flack and G. Bernardinelli, *Chirality*, 2008, **20**, 681–690; H. D. Flack and G. Bernardinelli, *Acta Crystallogr., Sect. A: Found. Crystallogr.*, 1999, **55**, 908–915; H. D. Flack, *Acta Crystallogr., Sect. A: Found. Crystallogr.*, 1983, **39**, 876–881.
51 L. Braunschweiler and R. R. Ernst, *J. Magn. Reson.*, 1983, **53**, 521–528.
52 A. D. Bain, E. P. Mazzola and S. W. Page, *Magn. Reson. Chem.*, 1998, **36**, 403–406.
53 J. Jeener, B. H. Meier, P. Bachmann and R. R. Ernst, *J. Chem. Phys.*, 1979, **71**, 4546–4553.
54 P. L. Rinaldi, *J. Am. Chem. Soc.*, 1983, **105**, 5167–5168.
55 A. Bax and M. F. Summers, *J. Am. Chem. Soc.*, 1986, **108**, 2093–2094.